Quantitative theory for electron-nuclear energy sharing in molecular ionization

Hao Liang ⬤[1] and Liang-You Peng ⬤[1,2,3,4,*]

[1]*State Key Laboratory for Artificial Microstructure and Mesoscopic Physics, School of Physics, Peking University, Beijing 100871, China*
[2]*Nano-optoelectronics Frontier Center of the Ministry of Education and Collaborative Innovation Center of Quantum Matter, Beijing 100871, China*
[3]*Collaborative Innovation Center of Extreme Optics, Shanxi University, Taiyuan 030006, China*
[4]*Beijing Academy of Quantum Information Sciences, Beijing 100193, China*

The dynamics of molecules in strong laser fields is much more complicated than that of atoms. For example, molecules can break up through dissociative single ionization, in which the electronic dynamics and nuclear dynamics are strongly correlated with each other. In this work we develop a quantitative theory based on the strong-field approximation to describe the dissociative single ionization of a hydrogen molecule, which allows us to schematically investigate the electron-nuclear energy sharing in the dissociative and the nondissociative single ionization of H_2 induced by intense laser pulses. Under different parameters of the laser pulse, we are able to discuss various types of dynamics in the framework of energy sharing, such as bond softening, dynamical quenching, vibrational trapping, and inverse bond hardening. In particular, we find drastic differences in the electron-nuclear energy sharing for UV and IR pulses. The current theoretical framework can potentially be extended to examine other strong-field phenomena in which the dynamics of different particles are correlated.

I. INTRODUCTION

Due to the large mass difference between an electron and a nucleus, the correlation effect between them is a rather interesting topic in different fields. The most famous one is the electron-phonon coupling in the conventional superconductor described by the Bardeen-Cooper-Schrieffer theory [1]. For the gas-phase molecules exposed to strong laser pulses, the Coulomb explosion (CE) [2–4] and laser-induced electron diffraction [5,6] provide powerful tools to inspect the electron-nuclear correlation via the kinetic energy release (KER) spectrum and the photoelectron momentum spectrum, respectively. In the past few years, with the fast development of lasers with a high repetition rate and techniques of the coincident measurement, one can acquire the joint energy spectrum (JES) for the electron and nucleus and the energy sharing between them has attracted a great deal of attention for the experimentalists. For example, the JES has been measured in the dissociative single-ionization (DSI) channel of H_2 induced by an intense laser pulse in the ultraviolet (UV) region [7], in the infrared (IR) region [8], or in a combined two-color field [9,10]. Similar experiments have also been carried out for the CE channel [11] and in the frustrated double-ionization process [12]. In addition, there have been a few experimental measurements on the DSI channel of CO [13,14].

To examine theoretically the JES in H_2, the most accurate and direct way is to numerically solve the time-dependent Schrödinger equation (TDSE) for the two electrons and the two nuclei. However, this kind of full dimensional computation for H_2 in laser fields has only been possible for few-photon processes induced by short extreme ultraviolet (XUV) pulses [15,16]. Due to the large difference between the timescales of the electronic ionization and of the nuclear dissociation, there exists a well-known multistep model for strong-field dynamics of H_2. Specifically, the first electron is ionized by the laser pulse and then the electronic and nuclear dynamics of the residual H_2^+ in the presence of the laser field can be separately treated. In most of the previous theoretical works, the molecular processes of H_2 triggered by UV or IR pulses are usually treated using the Franck-Condon (FC) approximation [17]. The ionization of the first electron is usually regarded as an instantaneous event that only happens at the peak of the pump pulse [3,18–20]. The ionization rate can be calculated at a fixed internuclear distance using the molecular Ammosov-Delone-Krainov theory [21,22], and the nuclear wave function of H_2^+ created by the first ionization is regarded as a vertical transition process under the FC approximation. In many other works, different nuclear vibrational states were used as the initial states before the pulse arrived [23–25], which corresponds to the cold H_2^+ experiment [26]. After choosing appropriate initial conditions according to different schemes, the TDSE for H_2^+ can be solved for either the nuclear motion on the adiabatic potential energy curves [27] of the electronic states or the diabatic ones [28,29].

Based on the above different methodologies, fruitful discussions on the ionization and dissociation dynamics of H_2 and H_2^+ in strong laser fields have been made over the

─────────
*liangyou.peng@pku.edu.cn

past three decades (for a recent review see, e.g., [30]). With an increase of the laser intensity, the gap of the avoided crossing of the molecular potential curves will widen, leading to the one-photon dissociation accessible by the lower vibrational states and consequently a lower threshold of the KER. This phenomenon is called bond softening [31]. Whenever the motion of vibrational wave packets and the motion of adiabatic potentials are properly synchronized, the laser-induced dynamical quenching of the molecular dissociation may occur [3,32], in which case the dissociation rate may decrease when the instantaneous laser intensity increases. The zero-photon dissociation [24,33] in which the nucleus can dissociate with very low KER through net-zero photon absorption provides the most dramatic evidence of vibrational trapping and bond hardening. Recently, light-induced conical intersections [34–36] were discussed with new aspects of the rotational dynamics of molecular dissociation.

The above separate treatment works well for pump-probe experiments with a short pump pulse ($\lesssim$10 fs) but is invalid for most experiments in which the ionization and dissociation processes are induced by the same laser pulse with a relatively long pulse duration (>10 fs). Since the electron-nuclear correlation is ignored, one cannot acquire any information regarding the electron-nuclear energy sharing from those calculations. Classical trajectory Monte Carlo approaches [37–40] have also been used to investigate the recollision-induced dynamics of H_2, which hardly can be applied to deal with the electron-nuclear energy sharing since the absorption of photon energy is intrinsically a pure quantum effect. As mentioned earlier, the full-dimensional TDSE calculations for H_2 are only feasible for few-photon processes induced by short XUV pulses. Due to the limitation of computational resources, theoretical treatments dealing with the electron and nuclei simultaneously for the IR pulses have only been attempted through reduced-dimensional molecules with model potentials depending on many parameters [41–44].

In this work we develop a quantitative theory based on the strong-field approximation (SFA), which allows us to schematically investigate the dissociative single ionization of H_2 in intense IR fields. The SFA is a widely used approximate approach that can be easily evaluated with the saddle-point method to an analytical expression. In this way, we can remove the degrees of freedom of the ionized electron in the TDSE, while the correlation between the ionized electron and the residual H_2^+ is still preserved. The motion of H_2^+ is then treated as nuclear motion on the energy curves of the two lowest electronic states. Using our method, we discuss the effects of the peak intensity, the center frequency, and the duration of the pulse on the dissociative single ionization. We observe different phenomena in the energy sharing under different laser parameters, which can be interpreted through a picture of adiabatic Floquet states. Atomic units are used throughout this paper unless otherwise stated.

II. THEORETICAL METHODS

For the presentation of our theoretical framework, let us introduce the following notation: H_0 is the field-free Hamiltonian of H_2 and V_{int} represents the laser-matter interaction within the dipole approximation, which is explicitly given in

the velocity gauge by

$$V_{int}(t) = \left(\boldsymbol{p}_{e1} + \boldsymbol{p}_{e2} - \frac{\boldsymbol{p}_{N1} + \boldsymbol{p}_{N2}}{m_N} \right) \cdot \boldsymbol{A}(t)$$
$$+ (1 - 1/m_N)\boldsymbol{A}^2(t)$$
$$\approx (\boldsymbol{p}_{e1} + \boldsymbol{p}_{e2}) \cdot \boldsymbol{A}(t) + \boldsymbol{A}^2(t), \quad (1)$$

where m_N is the nuclear mass and $\boldsymbol{A}(t)$ is the vector potential of the laser pulse, which vanishes for $t \notin (t_i, t_f)$. In the present method, we neglect the Coulomb interaction between the ionized electron and the residual H_2^+, which is denoted by V_m. Under this approximation, the total Hamiltonian of the system can be written as $H_f = H_0 + V_{int} - V_m$, which is equal to the sum of the H_2^+ part $H_{H_2^+}$ and the part of the ionized electron $(\boldsymbol{p}_e + \boldsymbol{A})^2/2$, with $\boldsymbol{p}_e$ the momentum of the ionized electron. In the following, $U_X(t_2, t_1)$ will be used to represent the propagator from t_1 to t_2 under a Hamiltonian H_X, where X denotes one of the particular physical systems involved above.

A. Strong-field approximation

In this section we formulate our theoretical methods based on the strong-field approximation. We start from the Dyson equation of the propagator

$$U(t, t') = U_0(t, t') - i \int_{t'}^{t} U(t, \tau)V_{int}(\tau)U_0(\tau, t')d\tau, \quad (2)$$

$$U(t, t') = U_f(t, t') - i \int_{t'}^{t} U_f(t, \tau)V_m(\tau)U(\tau, t')d\tau. \quad (3)$$

The transition amplitude W from the ground state $|0\rangle$ of H_2 to a given nondissociative single-ionization state $|X, \boldsymbol{p}_e\rangle$ is given by

$$W = \langle X, \boldsymbol{p}_e|U(t_f, t_i)|0\rangle$$
$$= -i \int_{t_i}^{t_f} \langle X, \boldsymbol{p}_e|U(t_f, \tau)V_{int}(\tau)|0\rangle e^{-iE_0(\tau - t_i)}d\tau, \quad (4)$$

where E_0 is the ground-state energy of H_2 and $|X\rangle$ represents a dissociative or a bound state of H_2^+. If we further replace $U(t_f, \tau)$ with the right-hand side of Eq. (3) and ignore the second term (i.e., the first-order strong-field approximation), we then get

$$\langle X, \boldsymbol{p}_e|U(t_f, \tau) \approx \langle X, \boldsymbol{p}_e|U_{H_2^+}(t_f, \tau)e^{-iS(t_f, \tau)}, \quad (5)$$

with the classical action of the ionized electron given by $S(t_f, \tau) = \frac{1}{2} \int_{\tau}^{t_f} [\boldsymbol{p}_e + \boldsymbol{A}(s)]^2 ds$. Substituting Eq. (5) into Eq. (4), we arrive at

$$W = -i \int_{t_i}^{t_f} \langle X, \boldsymbol{p}_e|U_{H_2^+}(t_f, \tau)V_{int}(\tau)|0\rangle$$
$$\times e^{-iS(t_f, \tau) - iE_0(\tau - t_i)}d\tau. \quad (6)$$

It should be noted that, although we throw out the term related to V_m explicitly in Eq. (3), the electron–parent-core interaction is still present implicitly inside $U_0(\tau, t')$ in Eq. (3) in our method. It gives a definite energy of the ground state, and the energy conservation law holds if one deals with the full system quantum mechanically; thus the electron nuclear energy sharing can be consistently studied with the present method.
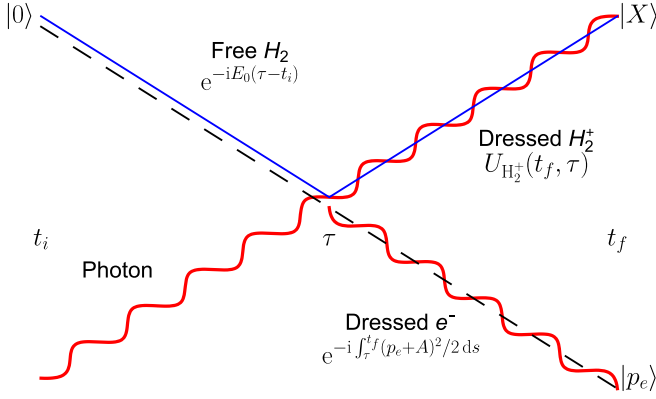
FIG. 1. Feynman diagram for our numerical scheme based on the strong-field approximation. The blue solid line, black dashed line, and red wavy line represent the hydrogen molecule ion, the electron, and the laser field, respectively.

Letting $\{|Y\rangle\}$ denote a complete orthonormal basis of H_2^+, we can introduce a projection operator $P = \sum_Y |Y, \boldsymbol{p}_e\rangle\langle Y, \boldsymbol{p}_e|$, which projects the system onto the subspace of the ionized electron with a momentum $\boldsymbol{p}_e$. Since V_m is neglected in our model and thus $U_{H_2^+}$ does not act on the ionized electron, we can insert P at the end of Eq. (5) to get

$$W = -i \int_{t_i}^{t_f} \langle X|U_{H_2^+}(t_f, \tau)|f(\tau; \boldsymbol{p}_e)\rangle d\tau, \qquad (7)$$

in which the function f is defined as

$$|f(\tau; \boldsymbol{p}_e)\rangle \equiv \sum_Y |Y\rangle\langle Y, \boldsymbol{p}_e|V_{\text{int}}(\tau)|0\rangle e^{-iS(t_f, \tau) - iE_0(\tau - t_i)}. \qquad (8)$$

In fact, the physical implication of Eq. (7) can be schematically shown by a Feynman diagram as in Fig. 1. The integration can be carried out through a numerical solution to the inhomogeneous TDSE of H_2^+,

$$[i\partial_t - H_{H_2^+}(t)]|\Psi(t)\rangle = |f(t; \boldsymbol{p}_e)\rangle, \qquad (9)$$

with the initial condition $|\Psi(t_i)\rangle = 0$. Finally, we can calculate the transition amplitude as $W = \langle X|\Psi(t_f)\rangle$. The fast oscillating phase factor of the inhomogeneous term in Eq. (8) can be removed by transforming the Hamiltonian into

$$H = H_{H_2^+} - \frac{1}{2}(\boldsymbol{p}_e + \boldsymbol{A})^2 + E_0. \qquad (10)$$

Through the procedures presented above, the degrees of freedom for the ionized electron have been removed from the TDSE and the electron-nuclear correlation can now be simply described through the parameter $\boldsymbol{p}_e$. In the following section we provide the details of the numerical realization, which allows us to systematically discuss the electron-nuclear energy sharing in the dissociative single ionization.

B. Numerical details

As a simple demonstration, we restrict ourself to include only the two lowest electronic states $|u\rangle$ and $|g\rangle$ of H_2^+ under the Born-Oppenheimer approximation. However, it is straightforward to consider more than these two states. In the present work, we only consider a linearly polarized laser pulse along the molecular axis. The length gauge is chosen

to describe the transition between these two states since the velocity gauge cannot give an accurate enough AC Stark shift in this restricted Hilbert space [45]. In this two-state model, the Hamiltonian of H_2^+ can be expressed as

$$H_{H_2^+}(t) = -\frac{1}{2M}\frac{\partial^2}{\partial R^2} + \begin{pmatrix} E_g(R) & \mu(R)F(t) \\ \mu(R)F(t) & E_u(R) \end{pmatrix}, \qquad (11)$$

where $M \approx m_N/2$ is the reduced mass, $E_u(R)$ and $E_g(R)$ are the energies of $|u\rangle$ and $|g\rangle$, respectively, at the internuclear distance R, and $\mu(R)$ is the corresponding transition dipole between the two states. Note that these three quantities can be numerically computed with our previous methods developed for H_2^+ in the fixed nuclear approximation [46]. The electric field strength of the laser pulse is given by $F(t) = -\partial_t A(t)$, with $A(t)$ the vector potential of the laser pulse. A similar framework has been presented by Gong *et al.* in a very recent work [47]; however, they did not discuss anything about the dynamics of the electron-nuclear correlation during the dissociative single ionization.

The singly ionized state $|Y, \boldsymbol{p}_e\rangle$ of H_2 is approximated as a symmetric product of a single electron bound state and a continuum state for H_2^+ computed from our previous fixed-nuclear code [46]

$$|Y, \boldsymbol{p}_e\rangle \approx \frac{1}{\sqrt{2}}(|Y\rangle_1 |\boldsymbol{p}_e\rangle_2 + |\boldsymbol{p}_e\rangle_1 |Y\rangle_2), \qquad (12)$$

since the ground state of H_2 is a singlet. The continuum state is normalized under the convention $\langle \boldsymbol{p}'_e | \boldsymbol{p}_e\rangle = \delta(\boldsymbol{p}'_e - \boldsymbol{p}_e)$. The ground state of H_2 can be expressed as a product of the electronic state computed from our numerical program for H_2 in the fixed nuclear approximation [48] and the corresponding vibrational ground state, i.e.,

$$\langle \boldsymbol{r}_1, \boldsymbol{r}_2, R|0\rangle \approx \Phi_0(\boldsymbol{r}_1, \boldsymbol{r}_2; R)\chi(R). \qquad (13)$$

Note that, since Eq. (8) is evaluated in the velocity gauge, we need to carry out a gauge transform of the electronic bound states.

To numerically solve Eq. (11), the R coordinate is discretized by the finite-element variable representation [49] in the range of [0, 40] a.u. In the results presented in the present work, 112 elements have been used with the Gauss-Lobatto quadrature of order 10, roughly corresponding to an average gird spacing around 0.036 a.u. A short-time propagator is used to evolve the wave function corresponding to the Hamiltonian (9), i.e.,

$$|\Psi(t + \Delta t)\rangle \approx e^{-i\overline{H}\Delta t}|\Psi(t)\rangle + \frac{e^{-i\overline{H}\Delta t} - 1}{-i\overline{H}}\overline{|f\rangle}, \qquad (14)$$

in which the overline represents a time average over the interval $(t, t + \Delta t)$. To evaluate both the exponent and the inversion of the Hamiltonian, we adopt a Krylov subspace technique [50] of order 40 and a time step Δt of 0.1 a.u.

The restarted Lanczos scheme [51] is used to find the possible final states including the vibrational states $|v\rangle$ ($v = 1, 2, \ldots$). The continuum states for different electronic states $|P_R, i\rangle$ ($i = g, u$) are evaluated by a direct solution to the ordinary differential equation, with the normalization condition $\langle P'_R, i'|P_R, i\rangle = \delta_{i,i'}\delta(P'_R - P_R)$. Therefore, the joint momentum distribution of the dissociative single ionization is

given by

$$P(\boldsymbol{p}_e, P_R) = \sum_{i=g,u} |\langle P_R, i | \Psi(t_f; \boldsymbol{p}_e) \rangle|^2, \qquad (15)$$

from which we can calculate the joint energy spectrum

$$P(E_e, E_R) = \sqrt{\frac{m_N E_e}{2 E_R}} \int P(\boldsymbol{p}_e, P_R) d\Omega_e \qquad (16)$$

by integrating over the angular variables. In the above formula, $E_R = P_N^2 / m_N$ and $E_e = \boldsymbol{p}_e^2 / 2$ are the kinetic energy release and the photoelectron energy, respectively. For the present case of a linear polarization, there is no dependence on the azimuthal angle ϕ_e and the integration over θ_e has been carried out by a Gauss-Legendre quadrature of order 10. In a similar way, the nondissociative single-ionization (NDSI) channel can be numerically evaluated; however, the details are omitted. In addition, a wave-function splitting technique [41] is used to avoid the reflection of the wave function near the grid boundary. All parameters have been carefully adjusted to ensure a full convergence of all the results.

III. RESULTS AND DISCUSSION

In this section we present and discuss our main results calculated at two different wavelengths of $\lambda = 395$ and 790 nm. We observe apparent changes of the JES for different intensities and durations of the laser pulse. In particular, the electron-nuclear energy sharing shows some distinct differences between the results at the two wavelengths.

In all the following calculations, we use a Gaussian laser pulse with a peak intensity of I_0 and a full width at half maximum (FWHM) of T_0. Note that the total duration of each pulse is taken to be $T_d = 6T_0$ to ensure an absolutely clean turn-on and turnoff of the laser pulse.

A. Results for λ = 395 nm

Let us first look at the results for a UV pulse with $\lambda = 395$ nm, whose JES is shown in Fig. 2 for various pulse durations T_0 of 7.0 [Fig. 2(a)], 20.2 [Fig. 2(b)], and 37.8 fs [Fig. 2(c)] and at different peak intensity I_0 of 5×10^{13} [Figs. 2(a i)–2(c i)] and 1.5×10^{14} W/cm² [Figs. 2(a i)–2(c iii)]. For a specific T_0 and I_0, the JES from the dissociative single ionization is shown in the upper part of each panel. In the lower part of each panel, we present the joint distribution of the vibrational states and the electron energy for the NDSI channel.

We can now examine a number of features in Fig. 2 and their changes as the increase of the duration and peak intensity of the pulse. One can draw a white dashed line for both DSI and NDSI channels according to the energy conservation in the multiphoton ionization process, i.e., $E_e + E_N = n\omega + E_0 - U_p$, where $U_p = I_0^2 / 4\omega^2$ is the ponderomotive energy at the peak intensity I_0. Since the ionization can occur in the entire duration of the pulse, one can observe that the actual joint distribution in both channels lies slightly above the white dashed line. As the pulse duration gets longer, the joint distribution becomes sharper due to a narrower spectral width of the pulse. An additional intriguing feature for the case of a longer pulse is that, for the NDSI channel, the vibrational
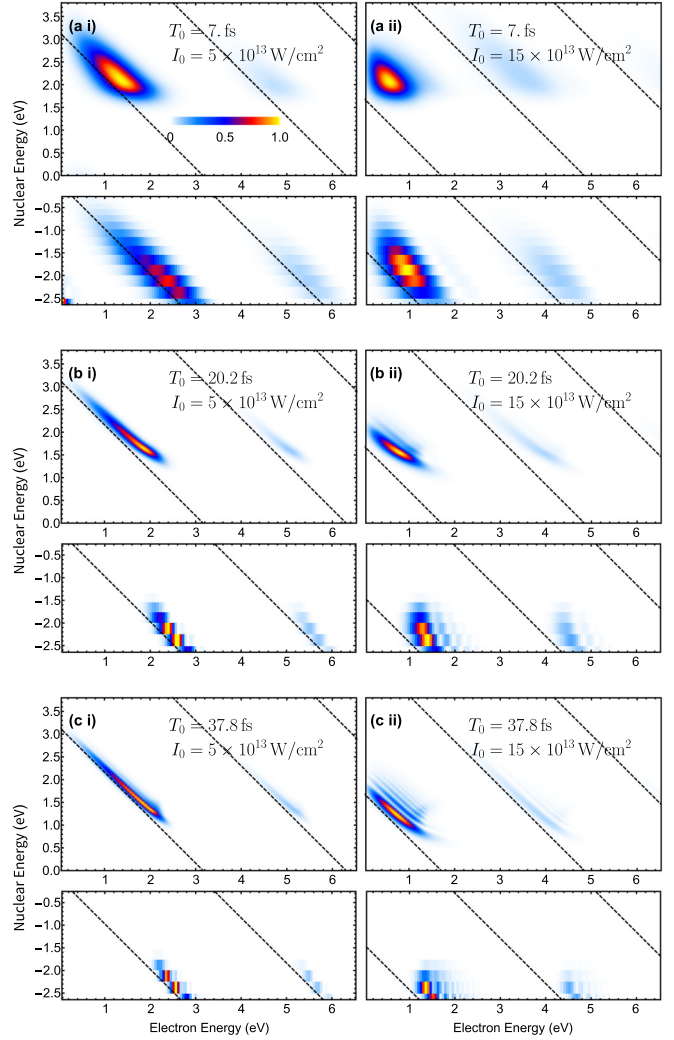

FIG. 2. Joint energy distribution for the dissociative single ionization (upper part in each panel) and the nondissociative single ionization (lower part in each panel) at a wavelength of $\lambda = 395$ nm in the UV region. Results are shown for two different peak intensities of 5×10^{13} W/cm² (left column) and 1.5×10^{14} W/cm² (right column) and three different pulse durations (a)–(c). In each panel, the white dashed line indicates the simple predication of the joint energy sharing relationship $E_e + E_N = n\omega + E_0 - U_p$ at the peak intensity of the pulse.

states with an energy above a certain threshold would not be bound anymore and will instead absorb one more photon and dissociate. This phenomenon will lead to a clear-cut upper boundary of E_N for the NDSI channel and a lower boundary for the DSI channel. As can be seen, this boundary decreases with an increase of the peak intensity, e.g., for $T_0 = 37.8$ fs, the boundary of the nuclear energy is about 1.3 eV for $I_0 = 5 \times 10^{13}$ W/cm² and 1.0 eV for $I_0 = 1.5 \times 10^{14}$ W/cm².

In fact, this phenomenon is known as dynamical dissociation quenching, observed many years ago in the total dissociation rate [3,32]. The quenching process can be easily understood based on the Floquet picture. For a monochromatic laser field, one can introduce a Floquet Hamiltonian at a fixed internuclear distance R and thus remove the time dependence
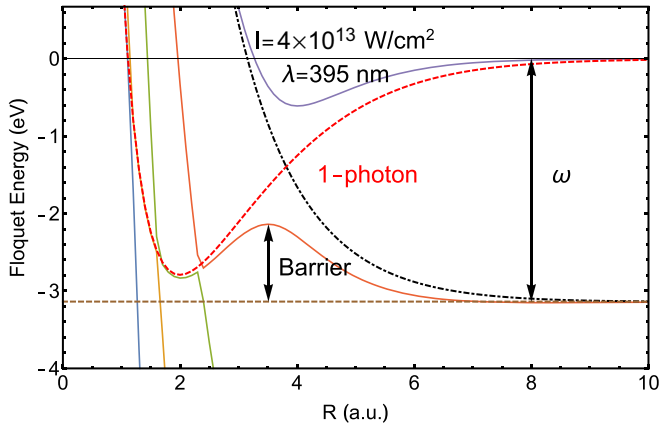
FIG. 3. Floquet energies of H_2^+ at $\lambda = 395$ nm and $I_0 = 4 \times 10^{13}$ W/cm^2. Solid lines are the energy curves for different Floquet states. The red dashed line represents the field-free energy curve for the $1s\sigma_g$ state, while the black dash-dotted line is for the field-free $2p\sigma_u$ state but shifted by one-photon energy.

of the laser field, i.e.,

$$H_F = \begin{pmatrix} E_g & 0 \\ 0 & E_u \end{pmatrix} + \frac{\hat{a} + \hat{a}^\dagger}{2} \begin{pmatrix} 0 & \mu F_0 \\ \mu F_0 & 0 \end{pmatrix} + \hat{N}\omega, \quad (17)$$

where F_0 is the electric field strength and $\hat{a}$, $\hat{a}^\dagger$, and $\hat{N}$ represent the annihilation, creation, and number operators of the photon field, respectively. By diagonalizing H_F, the Floquet energies can be evaluated as a function of R, as shown in Fig. 3. Comparing with the field-free case, one can see that the one-photon avoid crossing point creates one potential barrier for the lower curve and another potential well for the upper curve. Therefore, only the vibrational states with an energy higher than this barrier can absorb one more photon to dissociate, leaving those states with low energies remaining bound. As the intensity increases, this barrier will decrease, i.e., the bond softening will occur [52] so that the NDSI-DSI boundary will move towards a lower energy. Since the nucleus requires a time interval around 4 fs to move from the equilibrium internuclear distance $R \sim 1.4$ a.u. for H_2 to the position of the barrier around $R \sim 3.9$ a.u., the instantaneous intensity when the nucleus reaches the barrier must be smaller than the peak intensity, resulting a higher boundary. For a long pulse duration, these two intensities are not so different from each other; thus we conclude that the boundary goes lower as the pulse duration gets longer, which coincides with our numerical observations in Fig. 2 for a specific peak intensity.

Another distinct feature in Fig. 2 is that, for both the DSI and the NDSI channel, the curve of the joint distribution near the boundary bends upward, making it farther away from the white dashed line. It is a phenomenon driven by the laser envelope and can be understood as follows. Since the ionization rate exponentially depends on the actual laser intensity, we only consider the H_2^+ created near the peak of the laser envelope. For the nucleus with an energy near the barrier, the velocity is very slow when it reaches the barrier, and thus it will stay in this region for a significantly long time. As time goes on, the actual intensity will decrease

and thus the potential barrier will increase, which will give additional energy to the nucleus with an energy originally near the boundary. This type of bending effect can be observed even more clearly for intense IR pulses at $\lambda = 790$ nm, as will be shown later. A similar mechanism has been examined in a recent experiment of H_2^+ [53] based on the XUV pump plus IR probe.

We notice that the laser parameters used for Fig. 2(c i) are quite close to those in a previous correlation measurement [7]. The present theoretical results qualitatively agree with those observed in this experiment, which validates our present quantitative theory based on the SFA. For a better comparison, we replot the numerical results using the logarithmic scale in Fig. 6 to mimic the experiment data presented in Ref. [7]. We find that there are some differences, e.g., significant signals were experimentally observed in the low-KER region. These signals are mainly attributed to the effects of the excited states of H_2 [54], which are not considered in our present model.

Finally, for the JES in Figs. 2(b ii) and 2(c ii), we note that the distribution of the energy sharing shows a finer structure of parallel lines, which comes from the interference between different ionization events occurring in the rising and the falling part of the laser pulse due to the time-dependent AC Stark shift. A similar kind of peak splitting was first identified in the multiphoton detachment of H^- [55] and then rediscovered in the single-photon ionization [56,57] and multiphoton ionization [58] of neutral atoms.

B. Results for $\lambda = 790$ nm

In this section we turn to examine the case of IR pulses at $\lambda = 790$ nm. The joint distributions for both the DSI and NDSI channels are shown in Fig. 4 at four different intensities and for three different pulse durations. We find that these spectra become much more complex than those for $\lambda = 395$ nm. The most drastic difference is that, for the joint distribution of the one-photon DSI pathway, it does not follow the n-photon energy sharing line (the white dashed line); instead it stays in a narrow region of the KER, i.e., the distribution tends to be horizontal. This localized region of the KER is almost independent of the peak intensity, although it moves downward to a lower KER from around 0.8 eV to 0.2 eV with an increase of the pulse duration. For longer pulse durations at higher laser intensities, there even exists a positive correlation between the KER and the electron energy, as can be clearly seen in Figs. 4(c iii) and 4(c iv) for the one-photon DSI pathway. It seems that the nucleus gains some additional energy from the variation of the laser envelope, as we mentioned earlier for the UV laser case. In addition, the two-photon DSI pathway becomes dominant for laser pulses with longer duration and higher intensities [cf. Figs. 4(c iii) and 4(c iv)]. The time evolution of nuclear wave packets in the two electronic states is demonstrated in Fig. 7, where the different pathways can be roughly identified.

For the analysis of the joint distribution for the case of $\lambda = 790$ nm, we plot in Fig. 5 the Floquet energy curves at different laser intensities, as we have done for the 395-nm case. At rather low laser intensities, the energy curves are very similar to those of the 395-nm case, showing a barrier at one-photon crossing point. However, this barrier becomes
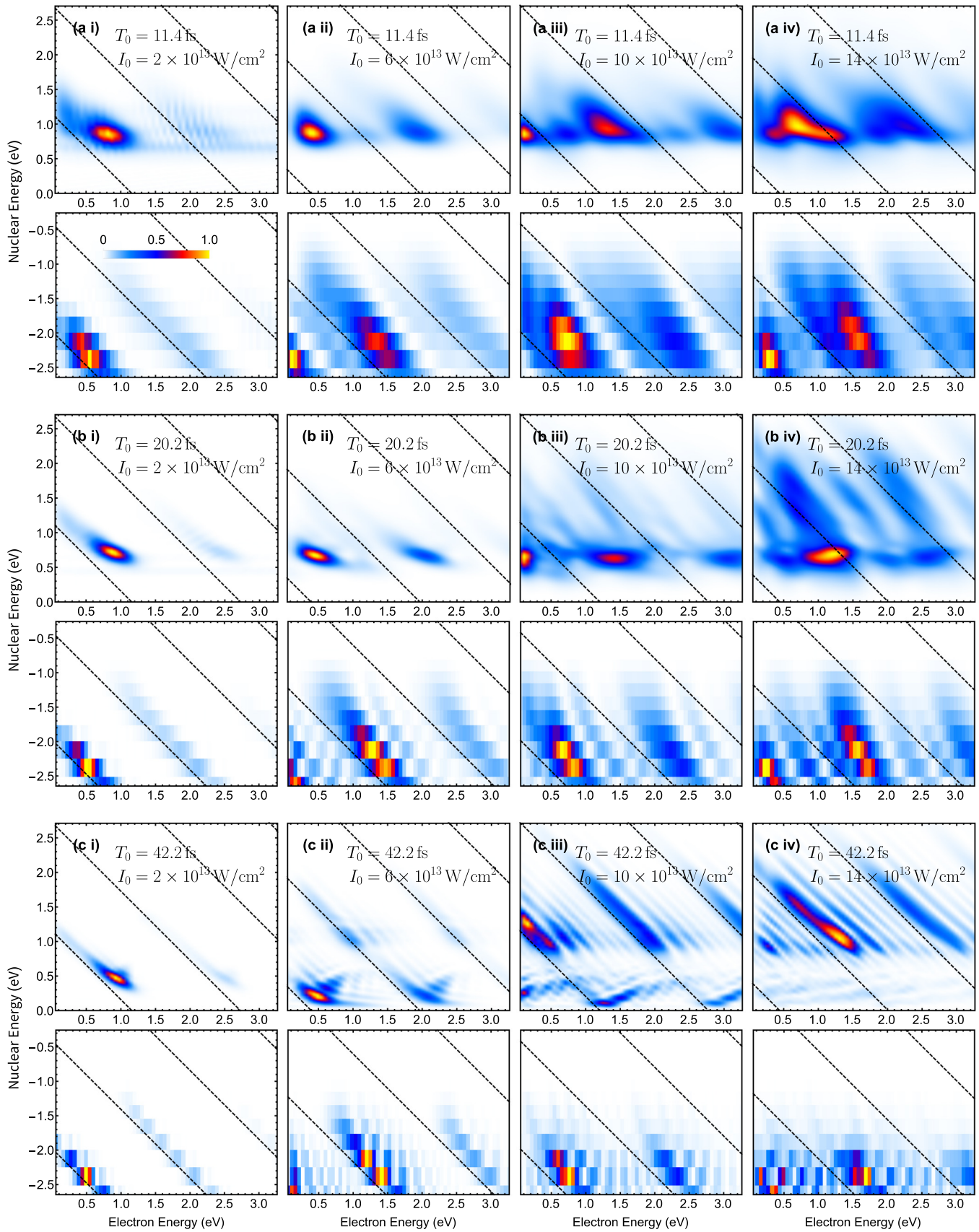
FIG. 4. Same as in Fig. 2 but for an IR pulse with $\lambda = 790$ nm at various peak intensities and pulse durations, as indicated in each panel.
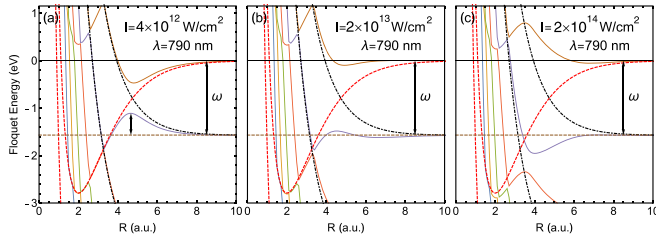
FIG. 5. Same as in Fig. 3 but for $\lambda = 790$ nm and an intensity of (a) 4×10^{12} W/cm^2, (b) 2×10^{13} W/cm^2, and (c) 1×10^{14} W/cm^2. These curves are periodic in energy with a period of 2ω.

flat for a moderate intensity of $I_0 = 2 \times 10^{13}$ W/cm^2 and even merges with the three-photon crossing point and forms a potential well at a higher intensity of $I_0 = 1 \times 10^{14}$ W/cm^2. This opens a new pathway, in which the nucleus absorbs three photons near the three-photon crossing point and then emits one photon near the one-photon crossing point. This expectation coincides with the clear diagonal lines of the energy sharing in the DSI channel, as shown in Figs. 4(c iii) and 4(c iv).

Now we try to understand the irregular distribution of the one-photon pathway. In the rising part of the pulse, the nuclear wave packets go through the three-photon crossing point and reach the internuclear region of 4 a.u. $\lesssim R \lesssim 6$ a.u. As the laser intensity reaches its maximum, the nearly flat energy curve changes into a potential well, which leads to the trapping of the nuclear wave packets with low kinetic energies (known as vibrational trapping in the literature [24,59]). Since the potential curve will rise again in the falling part of the pulse, the trapped wave packets will gain some additional energy and then dissociate or travel back to the region at small R, depending on their particular positions when the potential well rises. On the contrary, for trapped wave packets with higher kinetic energies, less energy will be gained in the last step since they travel faster when the pulse envelope varies. This explains the physical origin of the positive correlation between the KER and the electron energy for long pulse durations. At a relative low intensity of $I_0 = 4 \times 10^{12}$ W/cm^2, the vibrational trapping does not exist, while the nucleus can still gain some additional energy from the change of the pulse envelope, as discussed for the UV case of 395 nm. The mechanism mentioned here was first proposed by Frasinski *et al.* [60], referred to as bond hardening. Another name, inverse bond hardening, was assigned to it after its rediscovery by Hanasaki and Takatsuka [61]. In fact, we think the latter name is preferred since bond hardening usually refers to the suppressed dissociation of the high-lying vibrational states.

Finally, we notice that, for most of the laser parameters considered above, the ratio between the ponderomotive energy and the photon energy is greater than one (e.g., $U_p/\omega = 3.7$ for $I_0 = 10^{14}$ W/cm^2). A practical issue about the experimental observation should be emphasized here, i.e., most of the fine structures identified in our simulations will be washed out after the consideration of the focal volume effect [62]. This will allow only the gross patterns [63] to be experimentally observed, which coincides with existing experimental measurements [see, e.g., Fig. 6.5(b) in Ref. [64]].

IV. CONCLUSION

In summary, a quantitative numerical scheme based on the strong-field approximation has been developed to investigate the electron-nuclear joint energy spectrum for the dissociative single ionization and the nondissociative single ionization in H$_2$ induced by an intense laser pulse. Under the framework of our theory, we have discussed evidence of the bond softening, the dynamical quenching, the vibrational trapping, and the inverse bond hardening in the electron-nuclear energy sharing. A prominent energy exchange between the laser field and the molecular system driven by the pulse envelope was also found and discussed in the Floquet picture. In addition, the present theory allows us to quantitatively reproduce and understand most results in some previous experimental measurements.

The present theory may find applications in other possible strong-field processes in molecules. For the NDSI and the DSI channel, electron localization [9,65,66] and zero-photon dissociation [24,33] exist that can be discussed in the framework of the electron-nuclear energy sharing. After replacing the propagator of H$_2$$^+$ with a more accurate one [41,42], one can examine the correlation effect in the Coulomb explosion channel [8,11,12]. By including the second term in the Dyson series [67,68], it is possible to investigate the rescattering-induced process [2–4,69–71] in the molecular dissociation under the present scheme.

In general, our approach based on the strong-field approximation may provide an alternative tool for other correlated strong-field processes. By expanding the transition amplitude in terms of the interaction between the ejected electron and the residual ion, the dynamical variables are simply replaced by parameters and the difficulty in solving the TDSE can be largely reduced, while the entanglement between them is intrinsically preserved. This scheme is a resummation form of the intense-field many-body *S*-matrix theory [72] and can possibly find applications in the correlation effects in other systems, e.g., the sequential and nonsequential double ionization of helium [73].

APPENDIX A: COMPARISON WITH THE EXISTING EXPERIMENTAL MEASUREMENT

Here we replot our numerical results in logarithmic scale for a better comparison with the existing experiment measurement in Ref. [7]. As shown in Fig. 6, with an increase of the electron energy, the yield computed by our model decreases faster than that of the experimental result. This is not surprising since the SFA cannot reproduce a precise photoelectron spectrum, especially at a relatively-low-intensity region [74].
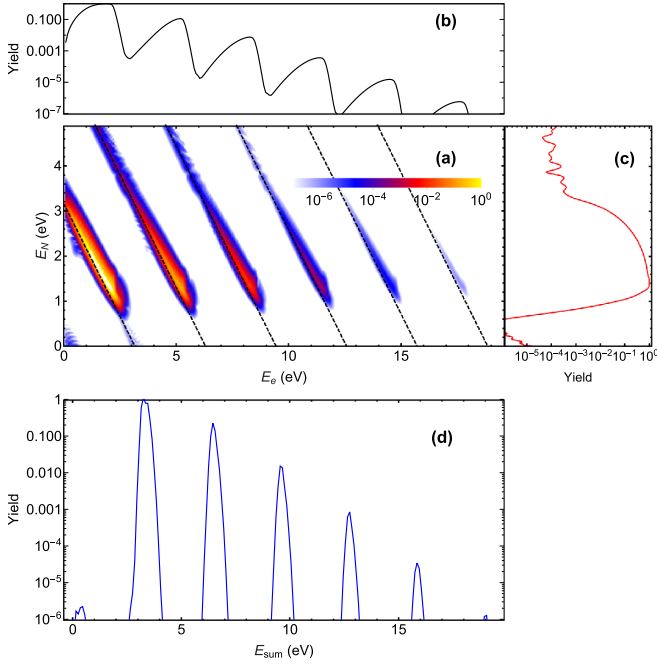
FIG. 6. Comparison with Fig. 4 in Ref. [7], with the laser parameters the same as those in Fig. 2(c i), (a) Electron-nuclear joint energy spectra of the dissociative single ionization plotted in logarithmic scale, (b) the corresponding electron energy spectrum, (c) the nuclear energy spectrum, and (d) the electron-nuclear sum-energy spectrum.

APPENDIX B: TIME EVOLUTION OF NUCLEAR WAVE PACKETS

We show the time evolution of the nuclear wave packets (NWPs) for selected laser parameters and electron momentum to help the reader have an intuitive picture of the dissociation. In Fig. 7 we plot $\rho_i(R, t) \equiv |\langle i, R|\Psi(t)\rangle|^2$ for $i = g, u$, which represents the time-dependent population of NWPs in the
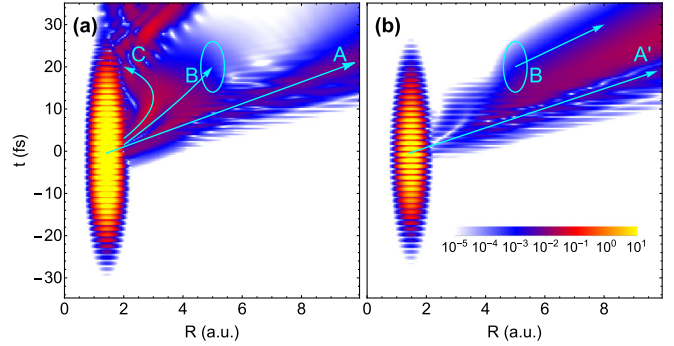

FIG. 7. Time evolution of the nuclear wave packets in the electronic states (a) $|g\rangle$ and (b) $|u\rangle$ for the laser parameters used in Fig. 4(a iii), i.e., a short FWHM of $T_0 = 11.4$ fs and a relative high peak intensity $I_0 = 10^{14}$ W/cm^2 with wavelength $\lambda = 790$ nm. The momentum of the ionized electron is chosen to be parallel to the molecular axis with amplitude $p_e \approx 0.35$ a.u. (with $E_e \approx 1.63$ eV).

electronic states $|g\rangle$ and $|u\rangle$, respectively. From Fig. 7 one can find that there is a large oscillation of the population in the FC region. It can be understood directly by looking at Eq. (9). However, this large oscillation precludes the possibility of visualizing the NWP near the FC region. The dissociation signal is dominated by the peak of the laser pulse for such a short pulse. After moving away from the FC region, there are three main channels for the NWPs: direct dissociation via a net two-photon (A) or three-photon (A') pathway, collision with the barrier and returning as a vibrational state (C), and being trapped near $R \approx 5$ a.u. and then dissociating in the falling part of the pulse envelope (B).

For the case of a long pulse duration (not shown here), there is a wider range of time for the birth of the NWPs. Due to the interference between the NWPs born at different times and different pathways, it is hard to get much useful information directly from the population evolution. It is possible to develop a semiclassical model for the nucleus to trace those pathways.

[1] L. N. Cooper, Phys. Rev. **104**, 1189 (1956).

[2] H. Niikura, F. Légaré, R. Hasbani, M. Y. Ivanov, D. M. Villeneuve, and P. B. Corkum, Nature (London) **421**, 826 (2003).

[3] H. Niikura, P. B. Corkum, and D. M. Villeneuve, Phys. Rev. Lett. **90**, 203601 (2003).

[4] H. Niikura, F. Légaré, R. Hasbani, A. D. Bandrauk, M. Y. Ivanov, D. M. Villeneuve, and P. B. Corkum, Nature (London) **417**, 917 (2002).

[5] M. Meckel, D. Comtois, D. Zeidler, A. Staudte, D. Pavičić, H. C. Bandulet, H. Pépin, J. C. Kieffer, R. Dörner, D. M. Villeneuve, and P. B. Corkum, Science **320**, 1478 (2008).

[6] B. Wolter, M. G. Pullen, A.-T. Le, M. Baudisch, K. Doblhoff-Dier, A. Senftleben, M. Hemmer, C. D. Schröter, J. Ullrich, T. Pfeifer, R. Moshammer, S. Gräfe, O. Vendrell, C. D. Lin, and J. Biegert, Science **354**, 308 (2016).

[7] J. Wu, M. Kunitski, M. Pitzer, F. Trinter, L. P. H. Schmidt, T. Jahnke, M. Magrakvelidze, C. B. Madsen, L. B. Madsen, U. Thumm, and R. Dörner, Phys. Rev. Lett. **111**, 023002 (2013).

[8] P. Lu, J. Wang, H. Li, K. Lin, X. Gong, Q. Song, Q. Ji, W. Zhang, J. Ma, H. Li, H. Zeng, F. He, and J. Wu, Proc. Natl. Acad. Sci. USA **115**, 2049 (2018).

[9] W. Zhang, H. Li, K. Lin, P. Lu, X. Gong, Q. Song, Q. Ji, J. Ma, H. Li, H. Zeng, F. He, and J. Wu, Phys. Rev. A **96**, 033405 (2017).

[10] Y. Mi, N. Camus, L. Fechner, M. Laux, R. Moshammer, and T. Pfeifer, Phys. Rev. Lett. **118**, 183201 (2017).

[11] P. Lu, W. Zhang, X. Gong, Q. Song, K. Lin, Q. Ji, J. Ma, F. He, H. Zeng, and J. Wu, Phys. Rev. A **95**, 033404 (2017).

[12] W. Zhang, X. Gong, H. Li, P. Lu, F. Sun, Q. Ji, K. Lin, J. Ma, H. Li, J. Qiang, F. He, and J. Wu, Nat. Commun. **10**, 757 (2019).

[13] W. Zhang, Z. Li, P. Lu, X. Gong, Q. Song, Q. Ji, K. Lin, J. Ma, F. He, H. Zeng, and J. Wu, Phys. Rev. Lett. **117**, 103002 (2016).

[14] X. Sun, M. Li, Y. Shao, M.-M. Liu, X. Xie, Y. Deng, C. Wu, Q. Gong, and Y. Liu, Phys. Rev. A **94**, 013425 (2016).

[15] A. Palacios, J. L. Sanz-Vicario, and F. Martín, J. Phys. B **48**, 242001 (2015).

[16] W.-Y. Wu and F. He, Sci. Rep. **8**, 14933 (2018).

[17] M. E. Wacks, J. Res. Natl. Bur. Stand. A **68A**, 631 (1964).

[18] T. Ergler, A. Rudenko, B. Feuerstein, K. Zrost, C. D. Schröter, R. Moshammer, and J. Ullrich, Phys. Rev. Lett. **97**, 193001 (2006).

[19] A. Staudte, D. Pavičić, S. Chelkowski, D. Zeidler, M. Meckel, H. Niikura, M. Schöffler, S. Schössler, B. Ulrich, P. P. Rajeev, T. Weber, T. Jahnke, D. M. Villeneuve, A. D. Bandrauk, C. L. Cocke, P. B. Corkum, and R. Dörner, Phys. Rev. Lett. **98**, 073003 (2007).

[20] F. Kelkensberg, W. Siu, J. F. Pérez-Torres, F. Morales, G. Gademann, A. Rouzée, P. Johnsson, M. Lucchini, F. Calegari, J. L. Sanz-Vicario, F. Martín, and M. J. J. Vrakking, Phys. Rev. Lett. **107**, 043002 (2011).

[21] T. Niederhausen and U. Thumm, Phys. Rev. A **77**, 013407 (2008).

[22] X. M. Tong, Z. X. Zhao, and C. D. Lin, Phys. Rev. A **66**, 033402 (2002).

[23] B. Feuerstein and U. Thumm, Phys. Rev. A **67**, 043405 (2003).

[24] A. Giusti-Suzor and F. H. Mies, Phys. Rev. Lett. **68**, 3869 (1992).

[25] F. Anis and B. D. Esry, Phys. Rev. A **77**, 033416 (2008).

[26] P. A. Orr, I. D. Williams, J. B. Greenwood, I. C. E. Turcu, W. A. Bryan, J. Pedregosa-Gutierrez, and C. W. Walter, Phys. Rev. Lett. **98**, 163001 (2007).

[27] A. D. Bandrauk and G. Turcotte, J. Phys. Chem. **87**, 5098 (1983).

[28] A. Abedi, N. T. Maitra, and E. K. U. Gross, Phys. Rev. Lett. **105**, 123002 (2010).

[29] A. Abedi, F. Agostini, Y. Suzuki, and E. K. U. Gross, Phys. Rev. Lett. **110**, 263001 (2013).

[30] H. Ibrahim, C. Lefebvre, A. D. Bandrauk, A. Staudte, and F. Légaré, J. Phys. B **51**, 042002 (2018).

[31] A. Zavriyev, P. H. Bucksbaum, H. G. Muller, and D. W. Schumacher, Phys. Rev. A **42**, 5500 (1990).

[32] F. Châteauneuf, T.-T. Nguyen-Dang, N. Ouellet, and O. Atabek, J. Chem. Phys. **108**, 3974 (1998).

[33] J. H. Posthumus, J. Plumridge, L. J. Frasinski, K. Codling, E. J. Divall, A. J. Langley, and P. F. Taday, J. Phys. B **33**, L563 (2000).

[34] A. Natan, M. R. Ware, V. S. Prabhudesai, U. Lev, B. D. Bruner, O. Heber, and P. H. Bucksbaum, Phys. Rev. Lett. **116**, 143004 (2016).

[35] P. Badankó, G. J. Halász, and Á. Vibók, Sci. Rep. **6**, 31871 (2016).

[36] M. Kübel, M. Spanner, Z. Dube, A. Y. Naumov, S. Chelkowski, A. D. Bandrauk, M. J. J. Vrakking, P. B. Corkum, D. M. Villeuve, and A. Staudte, arXiv:1906.08285.

[37] P. Dietrich, M. Y. Ivanov, F. A. Ilkov, and P. B. Corkum, Phys. Rev. Lett. **77**, 4150 (1996).

[38] A. Emmanouilidou, C. Lazarou, A. Staudte, and U. Eichmann, Phys. Rev. A **85**, 011402(R) (2012).

[39] A. Vilà, G. P. Katsoulis, and A. Emmanouilidou, J. Phys. B **52**, 015604 (2018).

[40] H. Price, C. Lazarou, and A. Emmanouilidou, Phys. Rev. A **90**, 053419 (2014).

[41] S. Chelkowski, C. Foisy, and A. D. Bandrauk, Phys. Rev. A **57**, 1176 (1998).

[42] F. He, A. Becker, and U. Thumm, Phys. Rev. Lett. **101**, 213002 (2008).

[43] Z.-C. Li and F. He, Phys. Rev. A **90**, 053423 (2014).

[44] J.-P. Wang and F. He, Phys. Rev. A **97**, 043411 (2018).

[45] A. D. Bandrauk, in *Frontiers of Chemical Dynamics*, edited by E. Yurtsever, NATO Advanced Studies Institute, Series C: Mathematical and Physical Sciences (Springer Netherlands, Dordrecht, 1995), Vol. 470, pp. 131–150.

[46] H. Liang, X.-R. Xiao, Q. Gong, and L.-Y. Peng, J. Phys. B **50**, 174002 (2017).

[47] X. Gong, P. He, J. Ma, W. Zhang, F. Sun, Q. Ji, K. Lin, H. Li, J. Qiang, P. Lu, H. Li, H. Zeng, J. Wu, and F. He, Phys. Rev. A **99**, 063407 (2019).

[48] W.-C. Jiang, L.-Y. Peng, J.-W. Geng, and Q. Gong, Phys. Rev. A **88**, 063408 (2013).

[49] T. N. Rescigno and C. W. McCurdy, Phys. Rev. A **62**, 032706 (2000).

[50] T. J. Park and J. C. Light, J. Chem. Phys. **85**, 5870 (1986).

[51] G. W. Stewart, *Matrix Algorithms*, 1st ed. (SIAM, Philadelphia, 2001), Vol. II .

[52] P. H. Bucksbaum, A. Zavriyev, H. G. Muller, and D. W. Schumacher, Phys. Rev. Lett. **64**, 1883 (1990).

[53] A. Fischer, M. Gärttner, P. Cörlin, A. Sperl, M. Schönwald, T. Mizuno, G. Sansone, A. Senftleben, J. Ullrich, B. Feuerstein, T. Pfeifer, and R. Moshammer, Phys. Rev. A **93**, 012507 (2016).

[54] X. Gong, P. He, Q. Song, Q. Ji, K. Lin, W. Zhang, P. Lu, H. Pan, J. Ding, H. Zeng, F. He, and J. Wu, Optica **3**, 643 (2016).

[55] D. A. Telnov and S.-I. Chu, J. Phys. B **28**, 2407 (1995).

[56] P. V. Demekhin and L. S. Cederbaum, Phys. Rev. Lett. **108**, 253001 (2012).

[57] M. Baghery, U. Saalmann, and J. M. Rost, Phys. Rev. Lett. **118**, 143202 (2017).

[58] R. Della Picca, A. A. Gramajo, C. R. Garibotti, S. D. López, and D. G. Arbó, Phys. Rev. A **93**, 023419 (2016).

[59] G. Yao and S.-I. Chu, Chem. Phys. Lett. **197**, 413 (1992).

[60] L. J. Frasinski, J. H. Posthumus, J. Plumridge, K. Codling, P. F. Taday, and A. J. Langley, Phys. Rev. Lett. **83**, 3625 (1999).

[61] K. Hanasaki and K. Takatsuka, Phys. Rev. A **88**, 053426 (2013).

[62] P. Hansch, M. A. Walker, and L. D. Van Woerkom, Phys. Rev. A **54**, R2559 (1996).

[63] C. He, H. Liang, M.-M. Liu, L.-Y. Peng, and Y. Liu, Phys. Rev. A **101**, 053403 (2020).

[64] Y. Mi, Strong-field ionization of atoms and molecules with two-color laser pulses, Ph.D. thesis, Ruperto-Carola-University of Heidelberg, 2017.

[65] D. Ray, F. He, S. De, W. Cao, H. Mashiko, P. Ranitovic, K. P. Singh, I. Znakovskaya, U. Thumm, G. G. Paulus, M. F. Kling, I. V. Litvinyuk, and C. L. Cocke, Phys. Rev. Lett. **103**, 223201 (2009).

[66] M. F. Kling, Science **312**, 246 (2006).

[67] A. Lohr, M. Kleber, R. Kopold, and W. Becker, Phys. Rev. A **55**, R4003 (1997).

[68] D. B. Milošević and F. Ehlotzky, Phys. Rev. A **57**, 5002 (1998).

[69] M. Busuladžić, A. Gazibegović-Busuladžić, D. B. Milošević, and W. Becker, Phys. Rev. Lett. **100**, 203003 (2008).

[70] B. Manschwetus, T. Nubbemeyer, K. Gorling, G. Steinmeyer, U. Eichmann, H. Rottke, and W. Sandner, Phys. Rev. Lett. **102**, 113002 (2009).

[71] X. M. Tong, Z. X. Zhao, and C. D. Lin, Phys. Rev. A **68**, 043412 (2003).

[72] A. Becker and F. H. M. Faisal, J. Phys. B **38**, R1 (2005).

[73] W. Becker, X. Liu, P. J. Ho, and J. H. Eberly, Rev. Mod. Phys. **84**, 1011 (2012).

[74] D. B. Milošević and W. Becker, Phys. Rev. A **99**, 043411 (2019).